

Fatigue performance monitoring of full-scale PPC beams by using the FBG sensors

Licheng Wang^{*1}, Jigang Han^{2a} and Yupu Song^{1b}

¹State Key Laboratory of Coastal and Offshore Engineering, Dalian University of Technology, Dalian, 116024, China

²Liaoning Provincial Communication Planning & Design Institute, Shenyang, 110179, China

(Received October 27, 2013, Revised March 9, 2014, Accepted April 14, 2014)

Abstract. When subjected to fatigue loading, the main failure mode of partially prestressed concrete (PPC) structure is the fatigue fracture of tensile reinforcement. Therefore, monitoring and evaluation of the steel stresses/strains in the structure are essential issues for structural design and healthy assessment. The current study experimentally investigates the possibility of using fiber Bragg grating (FBG) sensors to measure the steel strains in PPC beams in the process of fatigue loading. Six full-scale post-tensioned PPC beams were exposed to fatigue loading. Within the beams, the FBG and resistance strain gauge (RSG) sensors were independently bonded onto the surface of tensile reinforcements. A good agreement was found between the recorded results from the two different sensors. Moreover, FBG sensors show relatively good resistance to fatigue loading compared with RSG sensors, indicating that FBG sensors possess the capability for long-term health monitoring of the tensile reinforcement in PPC structures. Apart from the above findings, it can also be found that during the fatigue loading, there is stress redistribution between prestressed and non-prestressed reinforcements, and the residual strain emerges in the non-prestressed reinforcement. This phenomenon can bring about an increase of the steel stress in the non-prestressed reinforcement.

Keywords: partially prestressed concrete (PPC); FBG sensor; fatigue; monitoring; strain

1. Introduction

In recent years, partially prestressed concrete (PPC) has been widely used in bridges and offshore structures. These structures are subjected not only to static loading, but also to cyclic loading. Fatigue failure often occurs even if the applied load is well below the static capacity of the structures. Because of that, a lively interest in fatigue of PPC structures arises. With regard to the fatigue performance, numerous experiments have been undertaken on PPC beams (Bennett and Joynes 1977, Harajli and Naaman 1984, Shahawi and Batchelor 1986, Naaman and Founas 1989, Feng 2005, Zhang 2006, Yu *et al.* 2012). Fatigue failure mode has been identified as the fracture of tensile reinforcement in the beams. Obviously, in order to ensure the safety of the existing PPC

*Corresponding author, Associate Professor, E-mail: wanglicheng2000@163.com

^a Ph. D., E-mail: jiganghan@gmail.com

^b Professor, E-mail: syupu@dlut.edu.cn

structures under fatigue loading conditions, the best solution is to monitor the strain variation of the tensile reinforcement, and to assess the safety status in terms of the real-time information.

Based on the smart structure concept, fiber optic sensors have been successfully applied in various structural health monitoring (Kuang and Cantwell 2003, Li *et al.* 2004). Among several types of fiber optic sensors, e.g., the Fabry-Perot sensor, the fiber Bragg grating (FBG) sensor and the optical fiber time domain sensor, there has been growing recognition of the potential use of FBG sensors. Compared with other fiber optic sensors, the advantages associated with FBG sensors include long service life, resistance to electromagnetic interference, absolute measurement, multiplexing capability, and the added convenience of embedment (Chung and Kang 2008, Kim *et al.* 2011). These characteristics make FBG sensors an ideal candidate for sensing applications in civil and structural engineering such as bridges (Chan *et al.* 2006), high-rise buildings (Li *et al.* 2012), tunnels (Zhao and Qiu 2007) and dams (Zhu *et al.* 2010). It has been reported that the critical parameters of these structures which are able to be determined by FBG sensors include strain, displacement, crack width, temperature, etc (Merzbacher *et al.* 1996). Although FBG sensor systems have been widely studied and developed for monitoring large structures, existing systems may be limited by the technology available for any such application and often the use of high cost components (especially in optical interrogation systems) reduces their applicability, inevitably where budgets are limited (Kerrouche *et al.* 2009). In addition, harsh environmental conditions are often experienced and this can limit the ability of engineers to work on the installation and influence the durability of FBG sensor. Thus, its immaturity is evident in the need for improvements in grating fabrication and instrumentation, which will lower cost and standardize sensor system components. On the other hand, there is still a lack of conclusive information about sensor reliability and durability under different environmental and load conditions. Furthermore, there has been limited experience in the field with packaging, bonding and networking techniques for FBG sensors particularly on large structures. For these reasons, more research on the FBG sensors is needed.

Recently, the applicability of FBG sensors to the internal strain measurement in concrete structures was successfully verified through the steel strain monitoring in reinforced or prestressed concrete beams. For example, Davis *et al.* (1997) reported that FBG sensors were successfully used to measure the steel strains in reinforced concrete beams and deck panels when they were monotonically loaded to failure. Lin *et al.* (2004) presented experimental studies on strain measurements using embedded FBG sensors in a prestressed concrete beam. The experimental results indicated FBG sensors can be used to qualitatively monitor the structural integrity, from the time of concrete casting, throughout the service life of material. Kenel *et al.* (2004) embedded FBG sensors in reinforced concrete beams for strain measurements along reinforcing bars. The sensors were found to be capable of measuring large strains and strain gradients with high precision, but without significantly affecting the bond properties. Jacobs *et al.* (2007) studied the enhanced performance of dynamic monitoring of a prestressed concrete girder with FBG sensors. The obtained test results demonstrated the feasibility of FBG sensors, also for dynamic monitoring. Chung and Kang (2008) conducted a FBG sensing system to monitor the internal steel strains in the full-scale concrete box girder. It was found that the FBG sensing system can measure the dynamic properties as well as the internal strains. However, only little attention to date has been paid to the measurements of fatigue strain that truly responds to the working state of reinforced or prestressed concrete structures when subjected to fatigue loading until failure, upon the use of the embedded FBG sensors.

This paper aims to experimentally study the feasibility of using the embedded FBG sensors as a fatigue strain measuring device for the tensile reinforcement in PPC beams. For this purpose, full-scale post-tensioned PPC beams were made and tested under fatigue loading up to failure. Meanwhile, real-time monitoring of the strain variations of tensile reinforcement in the PPC beams was performed by using the embedded FBG and resistance strain gauges (RSG) sensors for the purpose of comparison of their results. Based on the monitoring data, the fatigue behavior of PPC beams is evaluated.

2. Principle of FBG sensors

The FBG is a spatially periodic modulation of the effective refractive index along a certain length of the core of an optical fiber. When a broadband light is launched into the FBG, a narrowband light is reflected due to Bragg diffraction and, as a result, is missing in the transmission spectrum (Taked *et al.* 2005).

The working principle of a FBG sensor is to monitor the shift in wavelength of the reflected spectrum with the changes in the measurand (e.g., strain, temperature), as shown in Fig. 1. According to Bragg’s law (Sante and Donati 2013), the reflective wavelength is expressed as:

$$\lambda_B = 2n_{eff} \Lambda \tag{1}$$

where λ_B is the Bragg wavelength; n_{eff} is the effective refractive index and Λ is the periodicity of the grating.

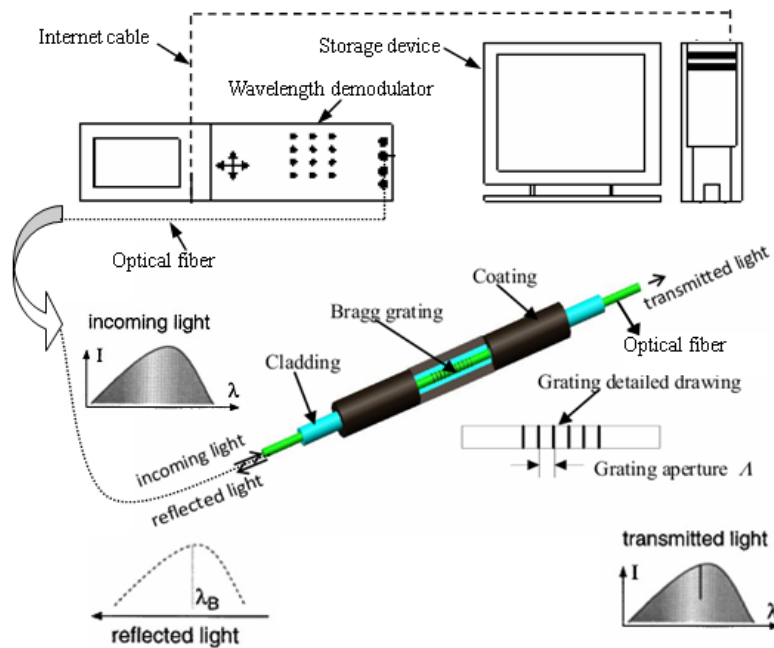


Fig. 1 Working principle and structure of FBG

As can be seen from Eq. (1), any change in the effective refractive index or the periodicity of the grating will change the Bragg peak wavelength. Consequently, any temperature or strain-induced effects on the FBG can be determined by the corresponding shift in the center Bragg wavelength. If we do not consider the effect of the coupling between the strain and temperature on FBG, the shift in Bragg wavelength with strain and temperature can be described by the following relation (Alan *et al.* 1997)

$$\frac{\Delta\lambda_B}{\lambda_B} = (1 - P_e)\Delta\varepsilon + (\alpha + \zeta)\Delta T \quad (2)$$

where $\Delta\lambda_B$ is the reflective Bragg wavelength shift; $\Delta\varepsilon$ is the strain shift; ΔT is the temperature shift; P_e is the effective photoelastic constant for fiber ($P_e \approx 0.22$); α and ζ are the thermal-expansion and thermo-optic coefficients, respectively ($\alpha + \zeta \approx 6.67 \times 10^{-6}$). Accordingly, based on Eq. (2), the strain can be determined by measuring the wavelength shift and the temperature shift.

3. Experimental program

3.1 Test specimens

The details of eight full-scale post-tensioned PPC beams are shown in Fig. 2. According to the different reinforcement arrangements, they were divided into two groups (Series H1 and H2). In each group, one beam, which was chosen as a reference beam for fatigue testing, was firstly tested monotonically up to failure in order to establish its ultimate bearing capacity, whereas others were tested under constant-amplitude fatigue loading until failure.

A locally available commercial concrete was used to cast the specimens. The time-dependent compressive strengths of concrete were experimentally determined at the time of beam testing (see Table 1). Prestressing was provided by seven wires strands. The initial prestressing force was equal to 1306 MPa, i.e., 70% of its specified ultimate strength. After post-tensioning, all beams were grouted. Two types of non-prestressed reinforcements were adopted, i.e., 14 mm and 16 mm in diameter respectively. Plain reinforcements with a diameter of 8 mm were used as the compressive reinforcement, and the shear reinforcement consisted of 6mm diameter stirrups. The properties of all steel reinforcements are listed in Table 2.

3.2 Loading scheme

An MTS hydraulic actuator of 1000 kN capacity was used for both monotonic and fatigue test. All beams were subjected to four-point loading, as shown in Fig. 3. The monotonic tests were conducted on two reference beams to determine their ultimate bearing capacity. For the fatigue test beams, prior to load cycling, they were first loaded statically to the maximum load (F_{max}) for two times. At this time the beams were initially precracked. After that, repeated loads were applied with the sinusoidal variation. The maximum load (F_{max}), the minimum load (F_{min}) and the cyclic loading frequency are all listed in Table 1. When the cycling number reached the predetermined intervals, the loading actuator was programmed to stop, and then the beams were unloaded to zero. Then a static load with a maximum value equaling to F_{max} was applied to the beam. Once this

process was completed, the fatigue loading was resumed. Fig. 4 shows the loading procedure.

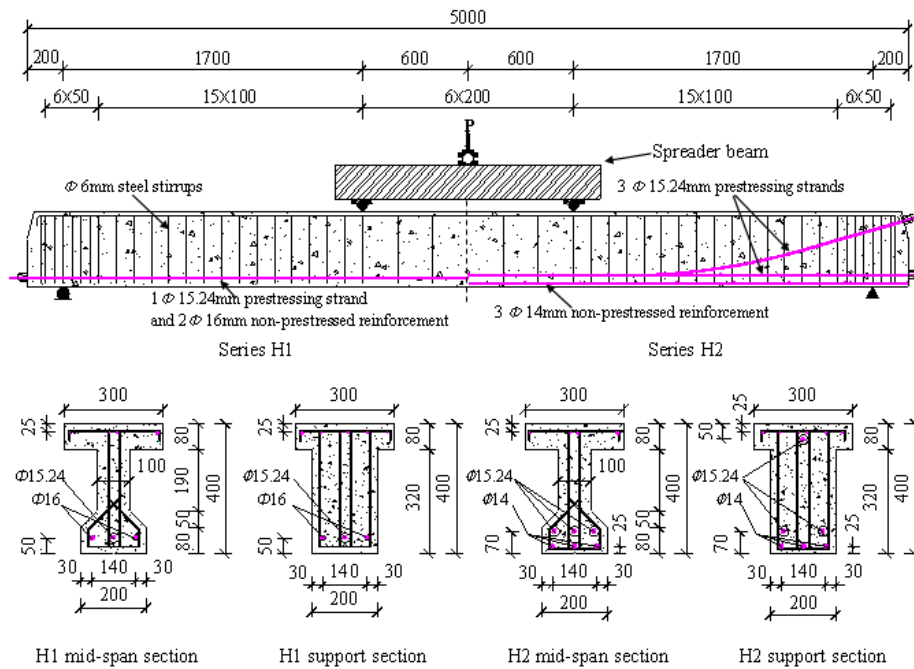


Fig. 2 Details of test specimens

Table 1 Summary of load parameters and experimental results

Beams ID	f_c^* (MPa)	load mode	Frequency (Hz)	F_{max}^* (kN)	F_{min}^* (kN)	F_u^* (kN)	N_f^*	Failure mode
H1S	55	Static				181		A
H1F-0.4	58	Fatigue	2	72	9		881228	B
H1F-0.5	61	Fatigue	2	91	9		208104	B
H1F-0.6	58	Fatigue	2	109			98320	B
H2S	54	Static				351		A
H2F-0.4	57	Fatigue	2	140	17		983245	B
H2F-0.5	59	Fatigue	1.5	176	17		384438	B
H2F-0.6	62	Fatigue	1	211	18		288190	B

* f_c : Concrete compressive strength; F_{max} : Maximum load; F_{min} : Minimum load; F_u : Ultimate bearing capacity; N_f : Fatigue life of beam. "A" represents yielding of steel reinforcement followed by crushing of concrete; "B" represents fracture of non-prestressed reinforcement. As for beams ID, "S" represents static test, "F" represents fatigue test, 0.4, 0.5, 0.6 after "F" represents the maximum load level (F_{max}/F_u).

Table 2 Properties of steel reinforcement

Reinforcement type	Diameter (mm)	Yield strength f_y (MPa)	Ultimate strength f_u (MPa)	Elastic Modulus $E_s(\times 10^5 \text{MPa})$
HRB400	16	413	642	1.94
	14	442	634	2.02
Strands	15.24	/	1867	1.96
HRB235	8	328	462	1.97
	6	347	477	1.96



Fig. 3 Test setup for monotonic and fatigue loading

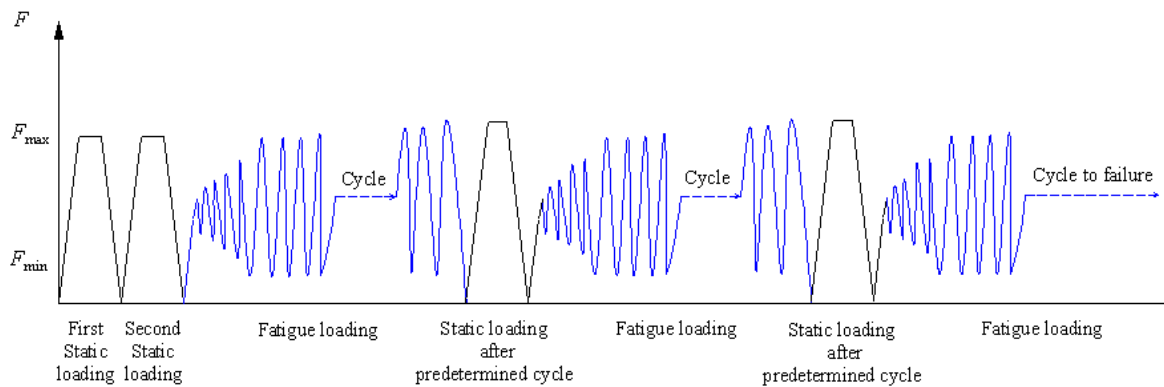


Fig. 4 Loading procedure for the fatigue test beams

3.3 Strain measurements and monitoring instrumentations

Strains in both the non-prestressed reinforcement and prestressing strands were measured by using the FBG sensors, including the single grating sensor and multiplexing sensors. Before casting concrete, these sensors were bonded onto the polished surface of tensile reinforcement with a specially selected and tested adhesive (ALTECO super glue adhesives), and then were protected with an epoxy resin layer, as shown in Fig. 5. Meanwhile, some resistance strain gauge (RSG) sensors were also installed in order to compare with strain response measured by the FBG sensors. Fig. 6 shows that the detailed arrangement of the FBG and RSG sensors along the length of tensile reinforcement. In addition, thermocouple probes were embedded into the test beams to monitor the temperature change, as well as to compensate for the temperature-induced wavelength shifts on the FBG sensors. After casting, one FBG sensor and one RSG sensor were adhered on the top concrete surface at the mid-span in order to measure the concrete strain in compressive region.

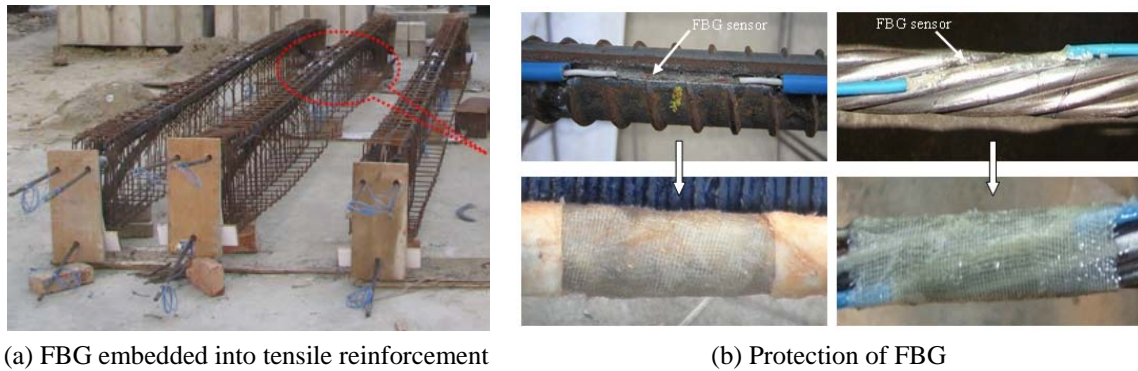


Fig. 5 Installation and protection of FBG sensors

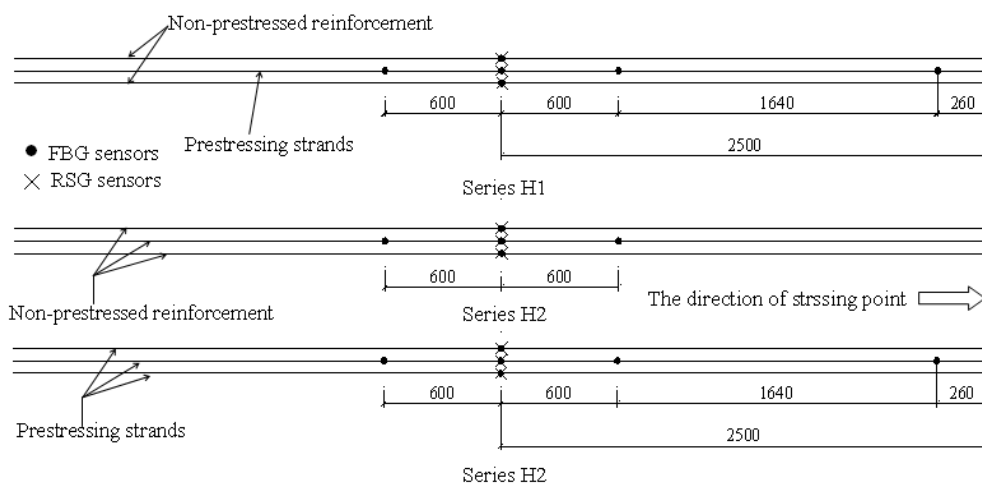


Fig. 6 Detailed arrangement of FBG and RSG sensors along the length of tensile reinforcement

The wavelength shifts induced by strain variation were continuously monitored in real-time by FBG sensors. The corresponding readings were acquired with the fiber-optic sensor measurement system which consisted of a multi-channel wavelength demodulator (a coupler and a storage device) (see Fig. 1). The readings of RSG sensors were recorded with an IMC data acquisition system. A temperature controller was connected directly to the thermocouple leads, which was used to obtain the temperature data.

4. Experimental results

4.1 Monitoring of the prestressing process

It is noted that positive and negative strain values denote tensile and compressive strains respectively. Prestressing strands in the test beams were post-tensioned by a load cell and an actuator. Tension force was applied in seven steps to the desired prestress level. Fig. 7 shows the strain variations in the prestressed and non-prestressed reinforcement measured by both the FBG and RSG sensors during prestressing, for beams H1F-0.6 and H2F-0.4, respectively. It is observed that there is a good consistency between the FBG and RSG measurements. Moreover, the compressive strain has been present in the non-prestressed reinforcement due to the prestressing effect. It can also be found that some RSG sensors failed prematurely, whereas none of FBG sensors were damaged.

For all test beams, the measured average initial prestress at the mid-span varied in the range of 1097 to 1277 MPa. After prestressing, these beams were stored in the laboratory for more than one year. During this time, due to the effect of elastic shortening, creep and shrinkage of the concrete, and relaxation of the prestressing strands, the measured average effective prestress correspondingly varied from 785 to 1010 MPa. At the same time, the compressive strains in the non-prestressed reinforcement also increased. It should be noted that an advantage of FBG sensors is that the sensed information (shift in wavelength) is an absolute quantity, and thus absolute strain measurements are obtained. In contrast, RSG sensors in this test only provide relative strain measurements. Therefore, the initial stresses/strains in the tensile reinforcement before loading tests were obtained from FBG sensors.

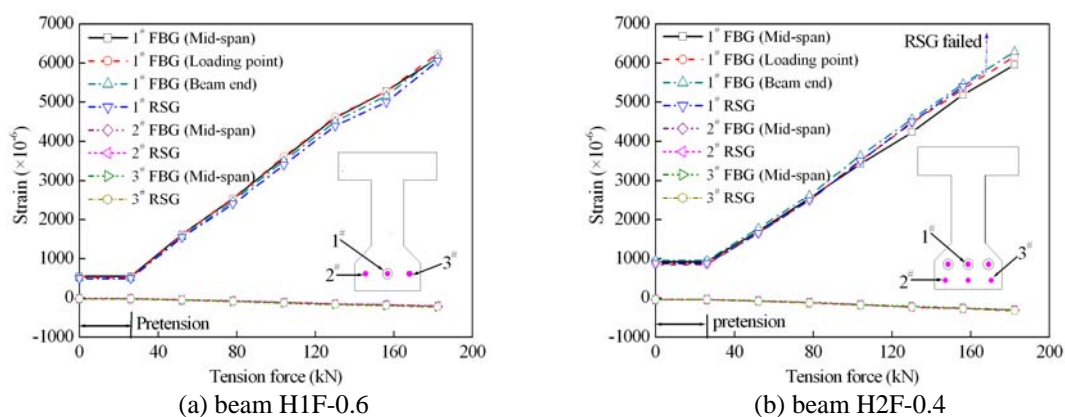


Fig. 7 Strain variation in the tensile reinforcement during prestressing

4.2 Strain measurements under fatigue loading

Prior to the fatigue tests, all beams were statically precracked. Fig. 8 shows the load-strain curves of the tensile reinforcement in beams H1F-0.4 and H2F-0.6 under the initial static loading. As can be seen in this figure, the strain responses show a sudden increase during loading. It implies that the main concrete crack has generated at the beam bottom. On the other hand, the results of FBG sensors are in close agreement with those recorded by the RSG sensors. This confirms that FBG sensors can be used in monitoring the internal steel strains in PPC beams under static loading conditions.

To verify the applicability of embedded FBG sensors under fatigue loading conditions, the strain ranges in the tensile reinforcement against the fatigue cycles are plotted in Fig. 9, which are separately obtained by using FBG and RSG sensors. Meanwhile, during fatigue loading, it is necessary to take into account the effect of the temperature shift in the tested beams on steel strain. Fig. 10 shows the temperature shift of beam H2F-0.5 in this process. Obviously, due to the effect of temperature difference between day and night, the measured temperature values vary from 17 to 21 °C. The similar temperature shift is shown by all the tested beams.

It can be seen from Fig. 9 that before the failure of RSG sensors, the consistency between the measurements of two sensors is satisfactory. More importantly, all the FBG sensors survived the fatigue tests while most of the RSG sensors failed in the procedure. This indicates that the FBG sensors are deemed capable of measuring the fatigue strain of the tensile reinforcement in PPC beams. As for RSG sensors bonded onto the tensile reinforcement in beams, their failure is mainly manifested by distortion of data. There are mainly two reasons for this. First of all, for the metallic wire-type strain gauges used in this paper, fatigue damage is evidenced as a permanent change in unstrained resistance of the RSG, ordinarily expressed in terms of equivalent indicated strain, and referred to as “zero-shift”. As damage increases in the RSG, cracks eventually begin to develop, and thus can result in data that is seriously in error. Secondly, it is more difficult to bond a RSG sensor to a polished surface of the tensile reinforcement than a FBG sensor. Bonding quality is also relatively poor. This can cause debonding of the securing point of RSG at higher strain range levels during fatigue loading.

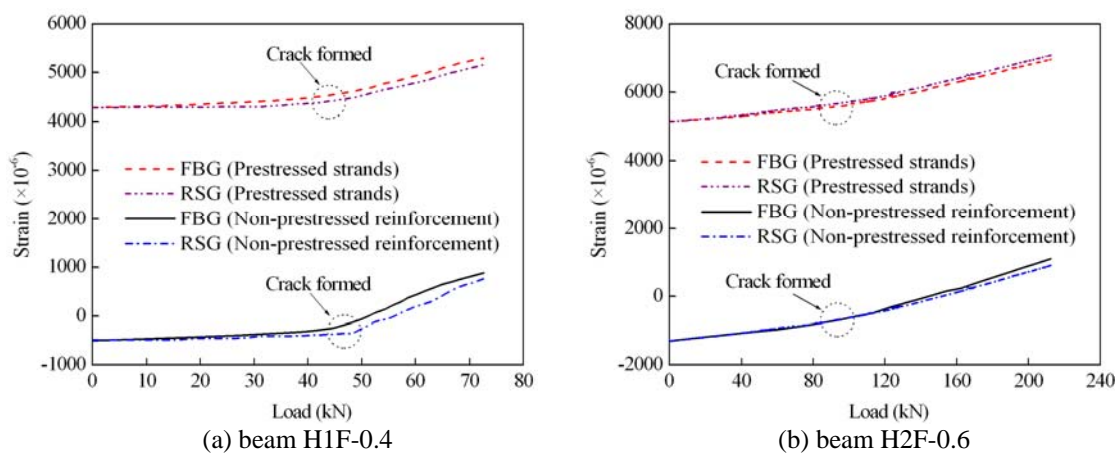


Fig. 8 Load-strain curves of the tensile reinforcement under the initial static loading

On the other hand, it can also be found that the strain ranges of the non-prestressed reinforcement are significantly higher than those of the prestressed strands, even for the beams of H1 series, in which the two different types of tensile reinforcement had been arranged in the same layer. This can be attributed to the fact that the bond mechanisms of prestressed and non-prestressed reinforcement with concrete are much different. This difference thus leads to the unsynchronized growth of stresses in the two types of reinforcements during fatigue loading, i.e., “steel stress redistribution”. Therefore, it can be concluded that the fatigue failure of PPC beam is initiated by the fracture of non-prestressed reinforcement, which has already been verified by the experimental results (see Table 1). From the viewpoint of practical monitoring, it is important to determine the strain state of the non-prestressed reinforcement in the beams under fatigue loading for the safety assessment of PPC beams.

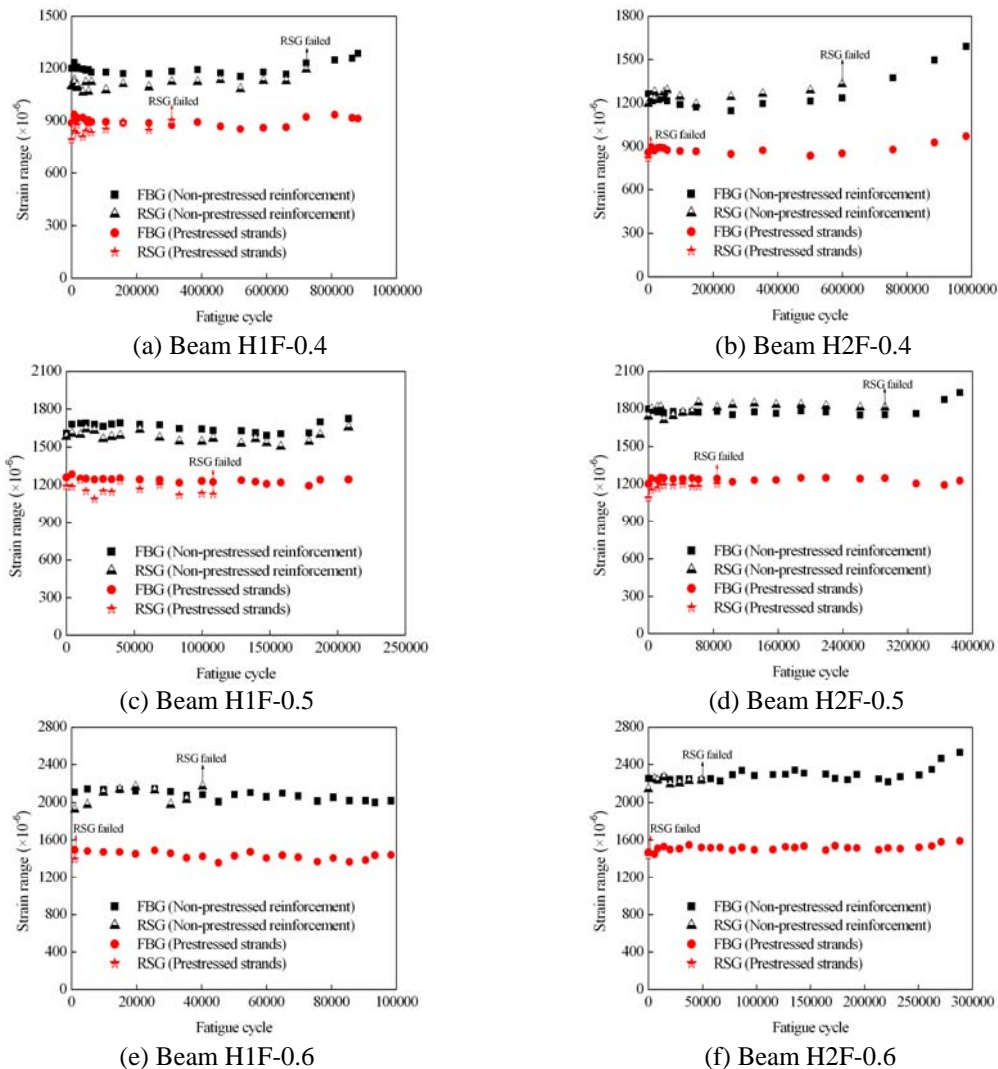


Fig. 9 Comparisons of the strain ranges between FBG and RSG sensors under fatigue loading

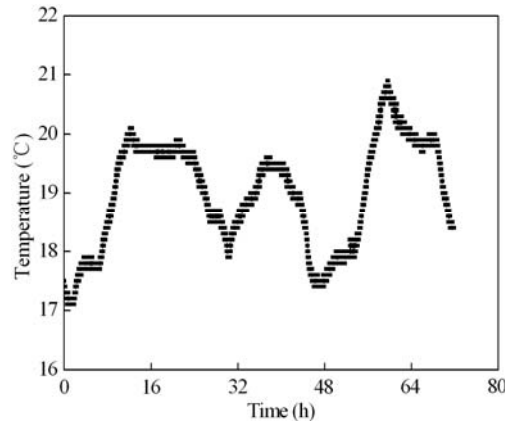


Fig. 10 Temperature shift in beam H2F-0.5 during fatigue loading

From the results obtained by using the FBG sensors, it is observed that except for beam H1F-0.6, there is an initial increase of the strain range in the non-prestressed reinforcement, continued by a stable stage where the strain range remains almost constant, and finally there is a sudden increase of strain range just before failure (see Fig. 9). The increase in strain range is usually attributed to the cycling creep and crack development of concrete. It should be noted that there is a rapid increase in strain range at the late stage of fatigue cycles, typically 15~20% before fracture of the reinforcement. This is regarded as a very important observation, since the upcoming failure may be detected by monitoring the strain in the non-prestressed reinforcement. Meanwhile, according to the monitored strain data, it can provide the stress profile that allows periodical evaluation of the fatigue life, and thus maintains a high level of safety of the structure.

As for beam H1F-0.6, the strain range remains constant throughout the whole test stage (see Fig. 9(e)). This is mainly due to the fact that the beam contains lower amount of non-prestressed reinforcement, which makes it difficult to resist the concrete crack development under a relatively larger F_{max} ($0.6F_u$), and hence the crack propagation has been completed at the early stage of fatigue cycling. Additionally, because of the lower fatigue life (only 98320 cycles), the cycling creep of concrete is relatively small.

Fig. 11 illustrates the comparisons of dynamic strains in the non-prestressed reinforcement obtained from FBG sensors during fatigue loading, including four sine waveforms. The sine waveforms were picked out respectively from the vibrating sine waveforms just before the stop of fatigue loading at the predetermined intervals. This figure shows that the maximum and minimum peak strains in the non-prestressed reinforcement increase with increasing of cycles. In addition, it can be also found that a residual strain occurs in the non-prestressed reinforcement after complete unloading. For example, for beam H1F-0.4, at 1000 fatigue cycles, there is -397×10^{-6} of steel strain after unloading. However, at 50000 and 700000 fatigue cycles, the residual strains are -279×10^{-6} and -239×10^{-6} , respectively. It implies that fatigue loading can induce the residual strain in the non-prestressed reinforcement, and thus lead to increase of the maximum and minimum peak strains. This phenomenon may be caused by either of the follow reasons: (1) the resistance of concrete to reverse slip at the interface between non-prestressed reinforcement and concrete; (2) the cracks can not close entirely when the beam is unloaded to zero (Harajli and Naaman 1984).

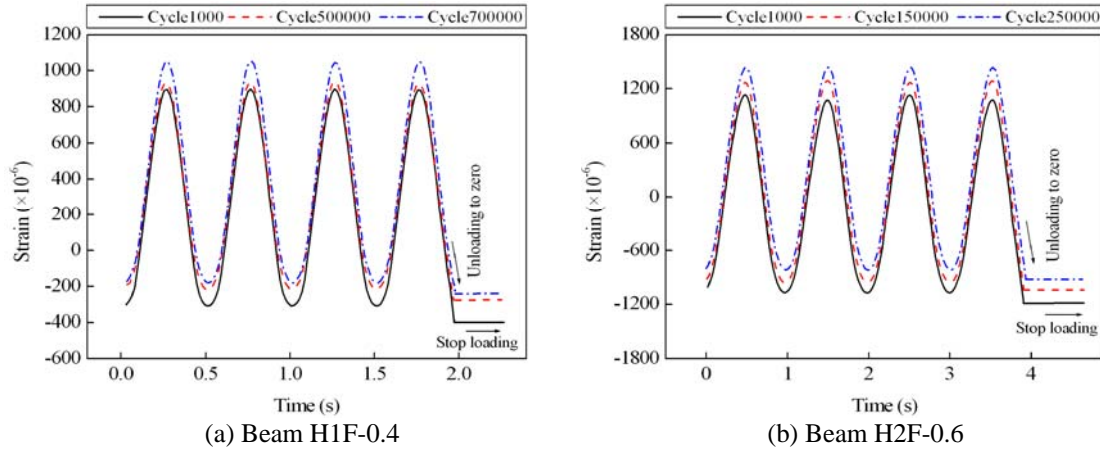


Fig. 11 Comparisons of dynamic strains in the non-prestressed reinforcement

Fig. 12 shows the strain history of the non-prestressed reinforcement in beam H1F-0.6 before failure. The strain was measured near the flexural cracks of concrete by FBG sensors. It can be seen that the strain of non-prestressed reinforcement experienced a sudden downward shift at failure. This phenomenon can be attributed to the retraction of non-prestressed reinforcement which is caused by its fatigue fracture in the main crack, as show in Fig. 13. After the fracture first occurred in the non-prestressed reinforcement, the deflections of beam and the strains in the other unbroken reinforcements show a significant increase. Although the beam can still sustain a certain number of load cycles, its ultimate bearing capacity and service performance decrease markedly during this time. In this case, strengthening or stiffening of the PPC beams is necessary in order to maintain their functionality.

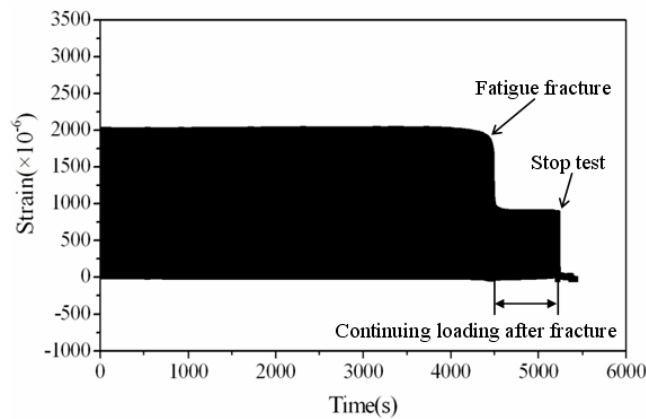


Fig. 12 Stroke history prior to failure of the non-prestressed reinforcement in beam H1F-0.6

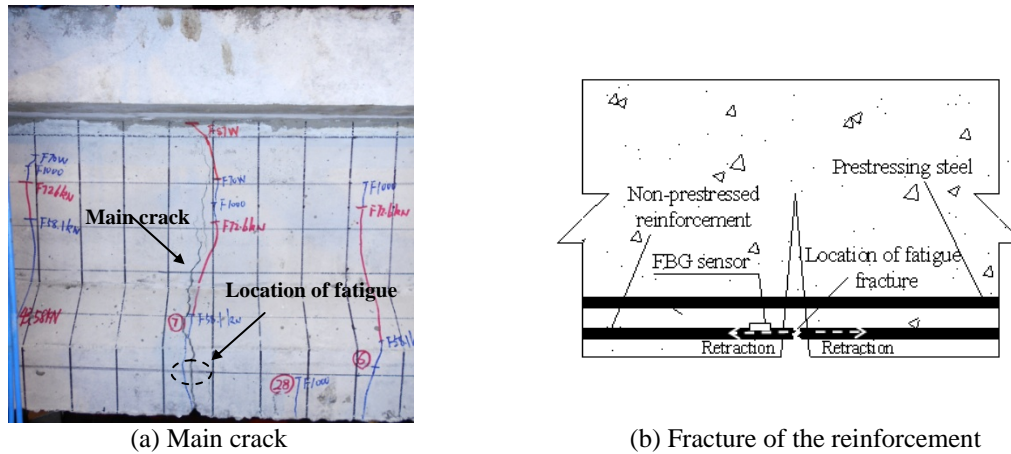


Fig. 13 Retraction of the non-prestressed reinforcement after fracture

5. Conclusions

To study the potential use of embedded FBG sensors for the real-time monitoring of steel strain in PPC structures under fatigue loading, fatigue tests were carried out on six PPC beams. The strains of tensile reinforcement in the beams were simultaneously measured by the embedded FBG and RSG sensors. According to the experimental results, several conclusions are summarized as follows:

- A good agreement between the measurements of FBG and RSG sensors is observed during the procedure of prestressing and fatigue loading. In addition, FBG sensors exhibit superior fatigue endurance and wider range of strain measurements compared with RSG sensors.
- FBG sensors have the potential for long-term health monitoring and improvement of inspection efficiency on large-scale PPC structures.
- Strain in the non-prestressed reinforcement can be used as a parameter to estimate the remaining fatigue life of PPC beams.
- Fatigue loading induces stress redistribution between prestressed and non-prestressed reinforcement, and the residual strain in the non-prestressed reinforcement. This can result in the increase of the non-prestressed steel stress, and thus increase the risk of fatigue failure of PPC beams. Thereafter, how to estimate the residual strain and to account for the effect of the stress redistribution on steel stress are open for investigation in the future work.

Acknowledgments

The research described in this paper was financially supported by the National High Technology Research and Development Program of China (863 Program) (Contract Number: 2007AA11Z133), the National Natural Science Foundation of China (No. 51378090) and the Fundamental Research Funds for the Central Universities of China (No. DUT14LK23).

References

- Alan, D.K., Michael, A.D., Patrick, H.J., LeBlanc, M., Koo, K.P., Askins, C.G., Putnam, M.A. and Friebele, E.J. (1997), "Fibre grating sensors", *J. Lightwave Technol.*, **15**(8), 1442-1463.
- Bennett, E.W. and Joynes, H.W. (1977), "Fatigue Resistance of reinforcement in partially prestressed Beams", *PCI J.*, **22**(2), 78-89.
- Chan, T.H.T., Yu, L., Tam, H.Y., Ni, Y.Q., Liku, S.Y., Chung, W.H. and Cheng, L.K. (2006), "Fiber Bragg grating sensors for structural health monitoring of Tsing Ma bridge: Background and experimental observation", *Eng. Struct.*, **28**(5), 648-659.
- Chung, W. and Kang, D. (2008), "Full-scale test of a concrete box girder using FBG sensing system", *Eng. Struct.*, **30**(3), 643-652.
- Davis, M.A., Bellemore, D.G. and Kersey, A.D. (1997), "Distributed fiber Bragg grating strain sensing in reinforced concrete structural components", *Cement. Concrete. Comp.*, **19**(1), 45-57.
- Feng, X.F. (2005), *Study on fatigue behavior of PPC beams with mixed reinforcement*, Ph.D. Dissertation, Dalian University of Technology, DaLian.
- Harajli, M.H. and Naaman, A.E. (1984), "Static and fatigue tests on partially prestressed beams", *J. Struct. Eng. - ASCE*, **111**(7), 1602-1618.
- Jacobs, S., Matthys, S., Roeck, G.D., Taerwe, L., Waele, W.D. and Degrieck, J. (2007), "Testing of a prestressed concrete girder to study the enhanced performance of monitoring by integrating optical fiber sensors", *J. Struct. Eng. - ASCE*, **133**(4), 541-548.
- Kenel, A., Nellen, P., Frank, A. and Marti, P. (2005) "Reinforcing steel strains measured by Bragg grating sensors", *J. Mater. Civil. Eng.*, **17**(4), 423-431.
- Kerrouche, A., Boyle, W.J.O., Sun, T. and Grattan, K.T.V. (2009), "Design and in-the-field performance evaluation of compact FBG sensor system for structural health monitoring applications", *Sensor. Actuat. A - Phys.*, **151**(2), 107-112.
- Kim, Y.S., Sung, H.J., Kim, H.W. and Kim, J.M. (2011), "Monitoring of tension force and load transfer of ground anchor by using optical FBG sensors embedded tendon", *Smart Struct. Syst.*, **7**(4), 303-317.
- Kuang, K. and Cantwell, W. (2003), "Use of conventional optical fibers and fiber Bragg gratings for damage detection in advanced composite structures: A review", *Appl. Mech. Rev.*, **56**(5), 493-513.
- Li, H.N., Li, D.S. and Song, G.B. (2004), "Recent applications of fiber optic sensors to health monitoring in civil engineering", *Eng. Struct.*, **26**(11), 1647-1657.
- Li, D.S., Ren, L., Li, H.N. and Song, G.B. (2012), "Structural health monitoring of a tall building during construction with fiber Bragg grating sensors", *Int. J. Distrib. Sens. N.*, **2012**(2012), 1-10.
- Lin, Y.B., Chang, K.C., Chern, J.C. and Wang, L.A. (2004), "The health monitoring of a prestressed concrete by using fiber Bragg grating sensors", *Smart. Mater. Struct.*, **13**(4), 712-718.
- Merzbacher, C.I., Kersey, A.D. and Friebele, E.J. (1996), "Fiber optic sensors in concrete structures: a review", *Smart. Mater. Struct.*, **5**(2), 196-208.
- Naaman, A.E. and Founas, M. (1991), "Partially prestressed beams under random amplitude fatigue loading", *J. Struct. Eng. - ASCE*, **117**(12), 3742-3761.
- Sante, R.D. and Donati, L. (2013), "Strain monitoring with embedded Fiber Bragg Gratings in advanced composite structures for nautical applications", *Measurement*, **46**(7), 2118-2126.
- Shahawi, M. and Batchelor, B. (1986), "Fatigue of partially prestressed concrete", *J. Struct. Eng. - ASCE*, **112**(3), 524-537.
- Taked, S., Minakuchi, S., Okabe, Y. and Takeda, N. (2005), "Delamination monitoring of laminated composites subjected to low-velocity impact using small-diameter FBG sensors", *Compos. Part A- Appl. S.*, **36**(7), 903-908.
- Yu, Z.W., Li, J.Z. and Song, L. (2012), "Experimental study on fatigue behaviors of heavy-haul railway bridges", *China Civil Eng. J.*, **45**(2), 115-126.
- Zhang, J.L. (2006), *Experimental study on fatigue behavior of Retard-bonded partially prestressed concrete beams*, Ph.D. Dissertation, Dalian University of Technology, DaLian.

- Zhao, X.G. and Qiu, H.T. (2007), "Application of fiber Bragg grating sensing technology to tunnel monitoring", *Chinese J. Rock Mech. Eng.*, **26**(3), 587-593.
- Zhu, H.H., Yin, J.H., Zhang, L., Jin, W. and Dong, J.H. (2010), "Monitoring internal displacements of a model dam using FBG sensing bars", *Adv. Struct. Eng.*, **13**(2), 249-262.